Molecular cloning, characterization, and expression of vacuolar-type-H⁺-ATPase B1 (*VHAB1*) gene in the gill of *Anguilla marmorata*

L. Li[1,2]*, Y.H. Jia[1,2]*, P. Li[1,2]*, S.W. Yin[1,2], G.S. Zhang[1,2], X.L. Wang[1,2], Y.Y. Wang[1,2] and X.J. Wang[1,2]

[1]Jiangsu Key Laboratory for Biodiversity and Biotechnology,
College of Life Sciences, Nanjing Normal University, Nanjing 3, China
[2]Co-Innovation Center for Marine Bio-Industry Technology of Jiangsu Province,
Lian Yungang, China

*These authors contributed equally to this study.
Corresponding author: S.W. Yin
E-mail: yinshaowu@163.com

ABSTRACT. We explored the molecular mechanism of the regulation of vacuolar-type-H⁺-ATPase B1 (VHAB1) in elvers in the response to salinity. The full-length cDNA of *VHAB1* in *Anguilla marmorata* (designated as *AmVHAB1*), which was 1741 base pairs (bp) in length, was found to encompass a 1512-bp open reading frame encoding a polypeptide with 503 amino acids (55.9 kDa), an 83-bp 5'-untranslated region, and a 146-bp 3'-untranslated region. The mRNA and protein expression levels of *AmVHA*B1 in the gill were evaluated at different time points (0, 1, 3, 6, 12, 24, 48, 72, and 96 h, and 15 days) during the exposure to various salinity levels (0, 10, and 25‰). The results indicated that the expression levels of *AmVHAB1* mRNA in the gill significantly increased and reached the highest level at 1 h exposure in the brackish water (BW, 10‰) group and at 6 h exposure in the seawater (SW, 25‰) group. The salinity level affected the relative

expression level of *AmVHAB1* mRNA in the gill, which was increased by approximately 44-fold in the SW group when compared with that in fresh water. Immunoblotting analysis showed that VHA expression was significantly higher in the BW and SW groups, with the highest expression level was detected at 96 h exposure. We found that the *AmVHAB1* gene in elvers from *A. marmorata* plays an important role in the adaptation to seawater.

Key words: *Anguilla marmorata*; Gill; mRNA and protein expression; Salinity; Vacuolar-type-H$^+$-ATPase

INTRODUCTION

Vacuolar-type-H$^+$-ATPases (V-H$^+$-ATPases) are membrane-bound multi-subunit enzymes that drive the unidirectional flow of protons across the plasma and organelle membranes (Wieczorek et al., 1999; Forgac, 2007). In recent years, V-H$^+$-ATPases have also been identified in lysosomes, endosomes, clathrin-coated vesicles, Golgi-derived vesicles, secretory vesicles, and the central vacuoles of yeast, neurospora, and plants (Bowman et al., 1992; Futai et al., 2000; Moriyama et al., 2000; Jefferies et al., 2008). V-H$^+$-ATPase, with a remarkably conserved molecular structure, is a heteromultimeric protein consisting of a catalytic V_1 domain involved in ATP hydrolysis, a 640-kDa complex containing 8 different subunits (A, B, C, D, E, F, G, and H), and a proton-conducting V_0 domain, which is a 250-kDa integral domain composed of 6 different subunits (a, d, e, c, c', and c") (Boesch et al., 2003a; Nelson, 2003; Forgac, 2007; Jefferies and Forgac, 2008). Hydrolysis of ATP can cause conformational changes in the catalytic A subunit that drive the rotation of subunits D and F of V_1. The subunit H can inhibit ATP hydrolysis in V_1 by bridging the rotor and stator stalks (Jefferies and Forgac, 2008). V- H$^+$-ATPase shares considerable structural similarity with ATP synthase.

The V-H$^+$-ATPase B1 gene (*VHAB1*) has been isolated from various teleostean fish, including European eel (Boesch et al., 2003b), zebrafish (Boesch et al., 2003a), and the rainbow trout *Oncorhynchus mykiss* (Perry et al., 2000), among others. A study of the European eel *Anguilla anguilla* showed that *VHAB1* in the bladder tissue shares structural features with the isoforms in the kidney of mammals, which are responsible for the extrusion of protons across the plasma membrane in several cell types (Niederstatter and Pelster, 2000; Cutler and Cramb, 2001). Immunocytochemical data showed that both isoforms of the B subunit from the European eel, based on significant staining, are observed in vesicles located near the apical membrane (Boesch et al., 2003b). A study in zebrafish indicated that 2 isoforms, *vatB1* and *vatB2*, share the greatest similarity to amino acid sequences of B subunits from the European eel *A. anguilla* and rainbow trout *O. mykiss* (Boesch et al., 2003a). In addition, a study in *Salmo salar* showed that the expression of the V-H$^+$-ATPase B subunit in the gill is upregulated during the early phase of smoltification, suggesting that V-H$^+$-ATPase is an important ion transporter that ensures ion uptake and is associated with changes in acid-base regulation during smoltification (Seidelin et al., 2001).

Anguilla marmorata (marbled eel; Osteichthyes, Anguilliformes, Anguillidae) is a typical catadromous migration fish and has a wide distribution throughout the tropical and subtropical western-central Pacific region (Shiao et al., 2003). Marbled eel can survive in both fresh water (FW) and seawater (SW) environments, with little change in the osmolality

of its body fluids, while elvers of *A. marmorata* must migrate from SW to FW for growth and development. Although the morphological development and growth environment of marbled eels have been well-studied, the molecular mechanisms of osmoregulation in eels are poorly understood. In this study, we cloned the full-length cDNA of *VHAB1* from juvenile *A. marmorata* (*AmVHAB1*). The biochemical and molecular changes associated with the adaptation to SW under controlled conditions were also investigated. This is the first report of the salinity adaptation of juvenile *A. marmorata*. Our results may be useful for exploring the molecular mechanism of osmoregulation in eels.

MATERIAL AND METHODS

Sampling

A. marmorata juveniles with a body mass of 1.99 ± 0.78 g and total body length of 10.95 ± 0.94 cm were obtained from the Hainan Island of South Sea, China. For the experiment, brackish water (BW, 10‰) and SW (25‰) were prepared from local tap water supplemented with the appropriate amount of synthetic sea salt (Aquarium Systems, Mentor, OH, USA). Eels were reared in FW (0‰) at 25°C with a daily 12-h photoperiod for more than 1 month before the experiments. The elvers were transferred to FW with a gradual increase in salinity of 2 each day until reaching BW and SW conditions. Eels were randomly anesthetized in an ice bath, and then the gill tissue was sampled from each salinity level (BW and SW) at 1, 3, 6, 12, 24, 48, 72, and 96 h, and 15 days after transfer for experiments (RNA isolation, immunoblotting). The control fish (FW, 0 h) were sampled before transfer. Throughout the experimental period, salinity and pH (range 6.5-7.5) were subjected to daily evaluation. The water was continuously circulated through fabric-floss filters, and fish were subjected to daily feeding with commercial pellets.

Cloning and sequence analysis of *VHAB1*

Total RNA from the gills of *A. marmorata* were prepared using Unizol reagent (Biostar, Shanghai, China) according to manufacturer instructions, and stored at -80°C. First-strand cDNA synthesis of *AmVHAB1* was performed following the manufacturer instructions using a gene-specific primer (VHA-GSP) and SuperScript™ II RT (Invitrogen, Carlsbad, CA, USA) as well as the 3'-CDS Primer A (3'-RACE-Ready cDNA). The detailed methods according to the manufacturer protocol were performed. All primers are shown in Table 1.

A fragment cDNA sequence from *AmVHAB1* of 277 base pairs (bp) was based on the known cDNA sequence of the European eel (*A. Anguilla*; AF179250.1). To amplify this cDNA fragment, 2 pairs of gene-specific primers (VHA-F/VHA-Fnest, VHA-R/VHA-Rnest) were designed to obtain the full-length cDNA of *AmVHAB1* by using 3' and 5' rapid amplification of cDNA ends (RACE). The 5' fragments of *AmVHAB1* were obtained using the 5'-RACE system for RACE Version 2.0 (Invitrogen) with gene-specific primers and the AUAP primer. The 3' fragment of *AmVHAB1* was amplified using the SMARTer™ RACE cDNA Amplification Kit (Clontech, Mountain View, CA, USA) using gene-specific primers (VHA-F/VHA-Fnest) and UPM. The full-length cDNA of *AmVHAB1* was obtained by overlapping the expression sequence tag with 5' and 3' fragments. All primers are listed in Table 1.

Table 1. Primers used for *AmVHAB1* gene cloning and real-time quantitative PCR quantification (F = forward primer; R = reverse primer).

	Primer names	Sequences (5'-3')
5'-RACE		
	VHA-GSP	TGCATACCTGGGGAAC
	VHA-R	GCCTTGGTTGTGAGATGTAG
	VHA-Rnest	TGCAGCTTCAGGTCCGTTGA
	AUPA	GGCCACGCGTCGACTAGTAC
3'-RACE		
	VHA-F	CTCACAACCAAGGCTGACATACTCCA
	VHA-Fnest	GCACCTGACCTTACCCGATGGCACC
	UPM-long	CTAATACGACTCACTATAGGGCAAGCAGTGGTATCAACGCAGAGT
	UPM-short	CTAATACGACTCACTATAGGGC
	3'-CDs primer A	AAGCAGTGGTATCAACGCAGAGTAC(T)30VN
ORF-QC		
	VHA-R-QC	CTATCGCTTGGGTGTCTTTGG
	VHA-F-QC	GCATTCTGGGAATTCGGCG
qRT-PCR		
	VHA-RT-F	GCCCAACGACATTAC
	VHA-RT-R	CTCCGACCACAGCCTTCA
	VHA-actin-F	GCAGATGTGGATCAGCAAGC
	VHA-actin-R	ACATTGCCGTCACCTTCATG

Homology analysis was accomplished using the online program BLAST at the National Center for Biotechnology Information. The open reading frame of *AmVHAB1* was determined using Open Reading Frame Finder, while the putative signal peptide was predicted using the SignalP 4.1 Server. Translation of *AmVHAB1* was performed using the DNAMAN software. Motif scanning was determined by a number of motif databases and the domain was scanned using the Simple Modular Architecture Research Tool. Potential N-glycosylation sites were predicted using the NetNGlyc 1.0 Server according to the Asn-X-Ser/Thr rule. The subcellular localization of the potential protein was predicted using the PRORT II server. The three-dimensional domain structure of AmVHAB1 was predicted using the SWISS-MODEL Server. Additional assessments of domain structures were performed using ProSA-Web and Verify3D Structure Evaluation Server. Phylogenetic analysis was also established using MEGA5.0 using the neighbor-joining method, and the reliability of branching was tested by bootstrap resampling (1000 pseudo-replicates). All analytical procedures and URLs are available in **Table S1**.

mRNA expression of ion transporter

The mRNA expression pattern of the gill *AmVHAB1* was analyzed using real-time polymerase chain reaction (PCR). The concentration of extracted total RNA was measured spectrophotometrically using the NanoDrop 2000 system (NanoDrop, Wilmington, DE, USA) and run on a 1% agarose gel to examine the quality and purity of RNA. Purified RNA with an A_{260}/A_{280} ratio between 1.8 and 2.0 was used for all RNA experiments. The first-strand cDNA synthesis of different samples for fluorescent real-time quantitative PCR (qPCR) analysis using HiScript™ QRT SuperMix was conducted using qPCR+gDNA wiper (Vazyme, Shanghai, China). qPCR was performed on a real-time thermal cycler Rotor-Gene Q (QIAGEN, Hilden, Germany). One pair of specific primers (VHA-RT-F, VHA-RT-R) was used to amplify the corresponding products of *AmVHAB1* from the cDNA template in qPCR

analysis. *AmVHAB1* transcript levels were normalized against β-actin (specific primers: VHA-actin-F and VHA-actin-R). The β-actin was expressed equally in all tissues tested. PCRs were conducted according to the manufacturer protocol of Faststart Universal SYBR Green Master (ROX) (Roche, Basel, Switzerland). All samples were subjected to PCR in triplicate. Melting curve analysis was performed after each reaction to confirm that only 1 fragment was amplified. Next, the qPCR data from 3 replicated experiments to ensure the accuracy and validity of experimental results were analyzed using the Rotor-Gene® Q Series Software (QIAGEN). The relative copy number of the target gene was calculated using the comparative C_t method with the following formula: $2^{-\Delta\Delta Ct}$ (Livak and Schmittgen, 2001). The data obtained from real-time PCR analysis were subjected to one-way analysis of variance (Wu and Hamada, 2000). P values were calculated by the Student *t*-test, and differences were considered to be significant when $P < 0.05$ and were considered to be highly significant when $P < 0.01$. Statistical analysis was performed using SPSS 17.0 for Windows (SPSS Inc., Chicago, IL, USA). All data are reported as the mean ± standard deviation in terms of relative mRNA expression.

Western blotting

The preparation procedure of crude membrane fractions from the gill tissues was performed according to the total protein extraction kit instructions (KeyGEN BioTECH, Nanjing, China). Protein concentrations were determined using the BCA Protein Assay Kit (KeyGEN BioTECH). The crude membrane protein fractions were stored at -80°C until immunoblotting experiments. The proteins from the membrane fractions were heated together with 2X sample buffer (125 mM Tris pH 6.8, 4% sodium dodecyl sulfate, 10% glycerol, 0.006% bromophenol blue, and 1.8% β-mercaptoethanol). All samples were separated by 7.5-12% sodium dodecyl sulfate-polyacrylamide gel electrophoresis and transferred to a polyvinylidene difluoride membrane (Millipore, Bedford, MA, USA). After pre-incubation for 1 h in phosphate-buffered saline containing 0.05% Tween-20 (PBS-T) containing 5% non-fat dried milk to minimize nonspecific binding, the samples were then incubated overnight at 4°C with a Atp6v1b2 polyclonal antibody against the rabbit VHA (GeneTex, Irvine, TX, USA) diluted in 1% bovine serum albumin and 0.05% sodium azide in PBS-T buffer (1:5000 dilution). After washing with PBS-T buffer, the samples were further incubated with a rabbit anti-mouse horseradish peroxidase-conjugated secondary antibody (diluted 1:5000) for 2 h at room temperature. The membranes were rinsed with PBS-T buffer again and the signal was detected using electrochemiluminescence and X-ray film (ECL Hyperfilm, GE Healthcare, Little Chalfont, UK). Immunoreactive bands were visualized using Renaissance chemiluminescence reagent (Perkin-Elmer Life Science, Waltham, MA, USA). In order to examine the amount of loading protein, the immunoblots were treated with stripping solution (62.5 mM Tris buffer, pH 6.7, containing 2% sodium dodecyl sulfate, and 100 mM β-mercaptoethanol) for 30 min at 50°C and incubated with mouse monoclonal anti-β-tubulin antibody (Sigma, St. Louis, MO, USA) followed by horseradish peroxidase-coupled goat anti-mouse IgG (Pierce, Rockland, IL, USA).

RESULTS

Identification and characterization of *VHAB1*

A 1741-bp nucleotide sequence, representing the full-length cDNA sequence of

AmVHAB1, was obtained by cluster analysis from the RACE-PCR-amplified fragments and the expressed sequence tags. The complete cDNA sequence was deposited in the GenBank database under the accession number KF932263. The full-length *AmVHAB1* cDNA includes an 83-bp 5'-untranslated region, a 1512-bp open reading frame encoding a 503-amino acid polypeptide, and a 146-bp 3'-untranslated region with a poly(A) tail (Figure 1). *AmVHAB1* shared significant similarity at the nucleotide level (80-98%) and at the protein level (91-99%) with the VHAB1 sequences reported in *A. anguilla* (99%), *Danio rerio* (97%), *Oncorhynchus mykiss* (97%), and *Maylandia zebra* (97%, B2 isoform). No signal sequence was identified in the transcript using the SignalP software. Protein domain scanning from the SMART diagram indicated that AmVHAB1 contains 3 domains, including an ATP-synt_ab_N domain (amino acid residues 41-107), an ATP-synt_ab domain (amino acid residues 163-390), and an ATP-synt_ab_C domain (amino acid residues 407-502) (shadowed areas in Figure 1). There were 3 potential *N*-glycosylation sites predicted for *AmVHAB1* (circled amino acid residues in Figure 1). A conserved amino acid motif defining the alpha and beta subunits of ATP synthase (ATP-synt_ab) belonged to the protein family signature PPINVLPSLS (amino acid residues 381-390 in Figure 1). Protein motif scanning results indicated that AmVHAB1 contains a functional region (amino acid residues 16-503). The predicted protein domain architecture of AmVHAB1 compared with other known VHAB1s from *A. anguilla*, *D. rerio*, *O. mykiss*, and *M. zebra* (subunit B2) was determined by SMART analysis. The results revealed that all VHAB1s share a similar domain structural pattern, all of which contain 3 domains (ATP-synt_ab_N, ATP-synt_ab, and ATP-synt_ab_C domains) (Figure 2). The three-dimensional structure of AmVHAB1 (Figure 3A) compared with VHAB1s from *A. anguilla* (Figure 3B), *O. mykiss* (Figure 3C), *M. zebra* (subunit B2) (Figure 3D), and *D. rerio* (Figure 3E) was determined using the SWISS-MODEL Server (Figure 3). The results indicated that AmVHAB1 and other known VHAβ1s share a common structural pattern. The three-dimensional structure of AmVHAB1 contains 14 antiparallel helices and 21 stranded β-sheets. Among these secondary structures, 9 highly twisted β-sheets are covered by α-helices. Some important structural motifs and nests such as Pro381, Val385, Leu386, Pro387, and Ser388 are located in the loop chain, while Pro382, Ile383, Asn384, Leu389, and Ser390 are located in β-sheets, forming the functional sites of the ATP/ATP synthase alpha and beta subunits. The Z-score of overall model quality was -10.09, and local model quality values for all residues were generally below 0 from ProSA-Web. The average 3D-1D scores from the Verify3D Structure Evaluation Server generally ranged from 0.03 to 0.69.

Phylogenic analysis of V-H⁺-ATPase B1

Phylogenic analysis was performed using the MEGA 5.0 software. The topology showed that *A. marmorata* and *A. anguilla* were clustered into one group, but the *D. rerio* V-H⁺-ATPase B1 shared a closer relationship with *A. marmorata* V-H⁺-ATPase when compared with *A. anguilla* V-H⁺-ATPase B2 (Figure 4). The topology of the phylogenic trees from amino acid datasets was similar to that of the nucleotide datasets with high bootstrap values and posterior probabilities. The conservative characteristics and high similarity with known *VHAB1s* confirmed that *AmVHAB1* belonged to the VHA family.

V-H⁺-ATPaseB1 mRNA and protein expression in the gill

The expression of *AmVHAB1* in the gill tissues of juvenile *A. marmorata* was tran-

siently increased to the highest level at 1 h post-transfer to BW and the highest level at 6 h post-transfer to SW (approximately 21.6- and 44.0-fold when compared to FW, respectively). After 3-24 h of SW exposure, the expression of *AmVHAB1* mRNA quickly reduced to a relatively lower level, but was still higher than that in the control fish group (Figure 5). Immunoblotting analysis showed that the gill VHA in BW and SW exhibited a single immunoreactive band with a molecular mass of approximately 33 kDa (Figure 6), and the protein expression levels of gill VHA in the BW and SW groups were significantly higher than that in the FW group. Similarly, the time point of the highest protein expression level of gill VHA in BW- and SW-acclimated eels occurred at 96 h, which was later than their highest mRNA expression time.

Figure 1. Nucleotide and deduced amino acid sequences of *VHAB1* from *A. marmorata*. The ATPase domains of VHAB1 are highlighted as shadowed areas. The protein family signature for the alpha and beta subunits of ATP synthase is shown in the open box. The potential *N*-linked glycosylation sites are labeled in the circle. The primers are indicated with arrows. The stop codon is labeled as *.
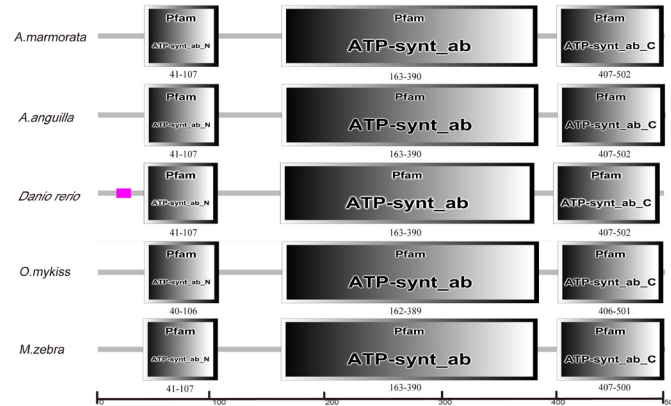
Figure 2. Predicted domain architecture of VHAB1 protein in *Anguilla marmorata* compared with *Anguilla anguilla*, *Danio rerio*, *Oncorhynchus mykiss*, and *Maylandia zebra* (subunit B2) was determined using SMART analysis. Low-complexity regions are labeled in pink and other domains are labeled accordingly.
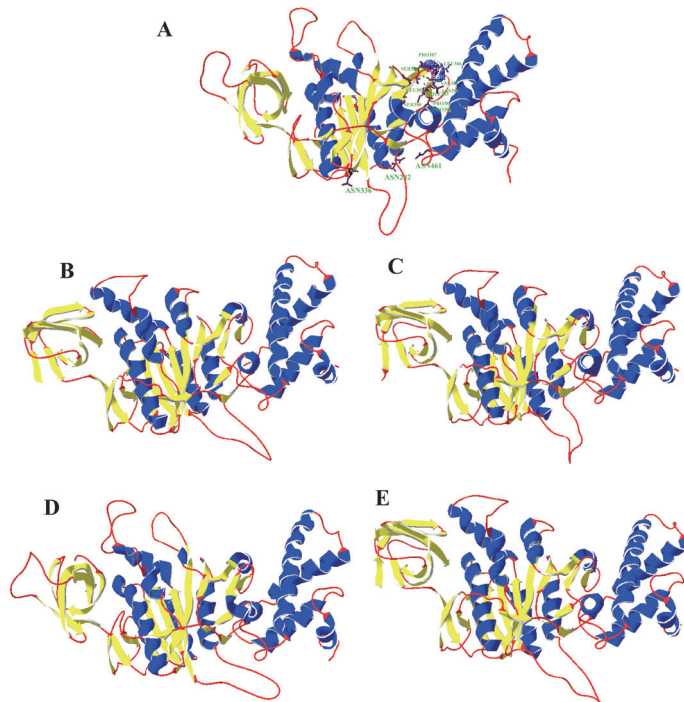
Figure 3. Structures of VHAB1 from 5 species. α-Helices (H) are labeled in blue, β-sheets (E) are labeled in yellow, and loops (C) are labeled in red. **A.** *Anguilla marmorata*, including 14 α-helices, 21 β-sheets, and 34 loops. Three-dimensional structures of the ATP synthase alpha and beta subunits are marked. Three formed *N*-glycosylation sites (Asn242, Asn336, and Asn461) are shown in purple. **B.** *A. anguilla*, including 12 H, 23 E, and 34 C. **C.** *Oncorhynchus mykiss*, 12 H, 23 E, and 35 C. **D.** *Maylandia zebra* (subunt B2), including 14 H, 21 E, and 34 C. **E.** *Danio rerio*, including 12 H, 23 E, and 34 C.
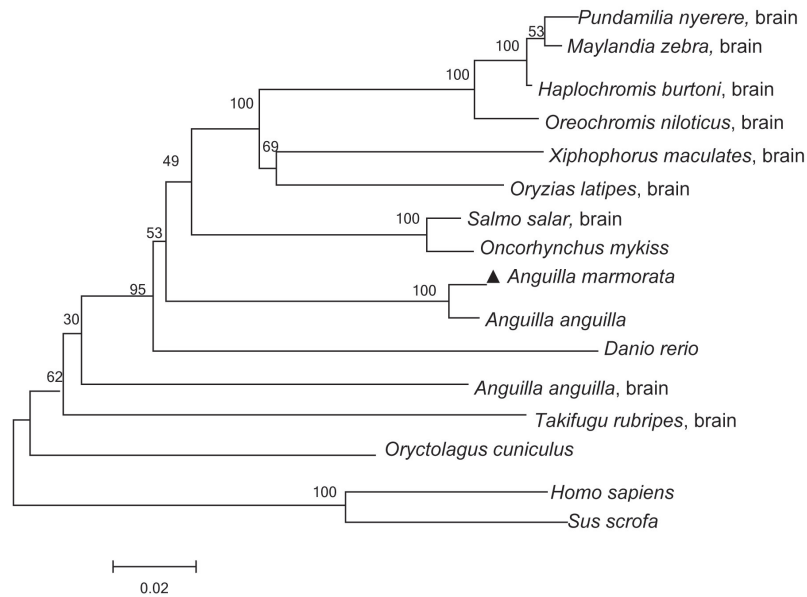
Figure 4. Unrooted neighbor-joining phylogenetic tree of *AmVHAB1* (triangle) and other vertebrates. Full-length amino acid sequences of *AmVHAB1* showed high similarity with other invertebrate *VHAs* in BLASTp homology searching. Numbers at the branch nodes indicate bootstrap values. The scale bar represents a branch length of 0.02 for amino acids.
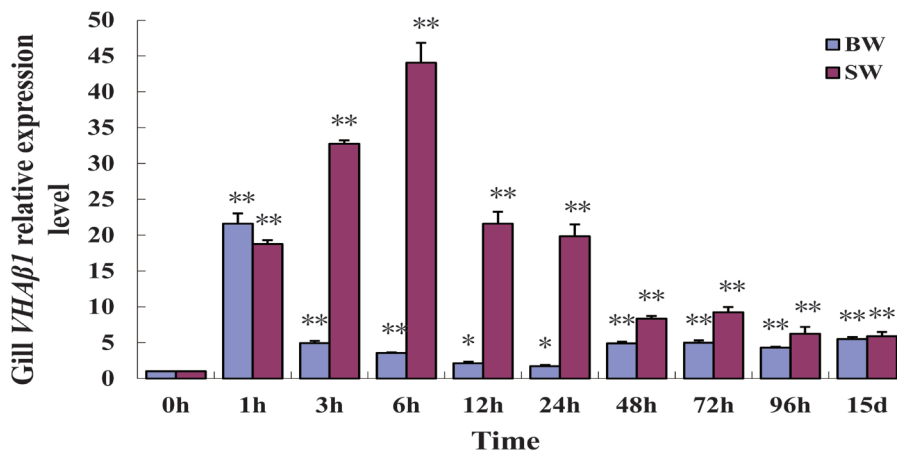
Figure 5. Time-course analysis of *AmVHAB1* expression pattern in the gill by real-time PCR caused by changes in salinity after transfer from brackish water (BW, 10‰) to seawater (SW, 25‰). The mRNA levels of *AmVHAB1* were analyzed and standardized according to β-actin mRNA levels. Error bars present as standard deviation of 3 independent measurements. Statistical significance was considered at *P < 0.05 and **P < 0.01 when compared with that of the control (freshwater: FW, 0 h), (N = 3, df = N - 1).
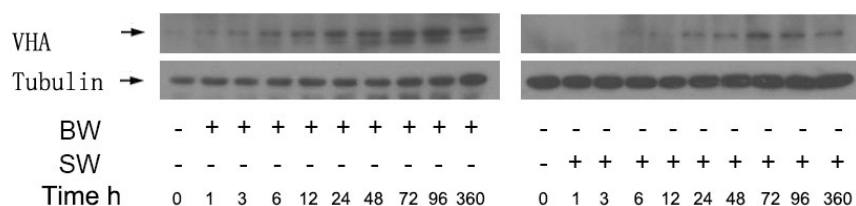
Figure 6. A representative immunoblot of gills from *Anguilla marmorata* in response to brackish water (BW) and seawater (SW) at 1, 3, 6, 12, 24, 48, 72, and 96 h, and 15 days of exposure to the salinity, which were probed with a primary antibody against V-H⁺-ATPase (Atp6v1b2) and confirmed as a single immunoreactive band with a molecular weight of approximately 33 kDa.

DISCUSSION

The maintenance of a stable internal environment is crucial for animals to survive in a variety of habitats. Ion-transporting epithelia in the gills and kidneys play important roles in modulating ion flux in response to changes in environmental salinity. In recent studies, an increasing amount of V-H⁺-ATPase isoforms was identified from teleosts, and shown to be involved in osmotic regulation. The full-length cDNA of *VHAB1* (possibly the kidney isoform) was cloned from the juvenile *A. marmorata* in this study. Conserved sequences and characteristic motifs, such as the protein family signature of alpha and beta subunits in ATP synthase, ATP-binding domain, and the major typical structural and functional domains in VHA (Leng et al., 1998; Boesch et al., 2003b; Reilly et al., 2011; Wang et al., 2012) were detected in the deduced AmVHAB1 amino acid sequences from *A. marmorata*, suggesting that *AmVHAB1* is functional. VHAB1 is the partial head region of the protein and is not a transmembrane protein, which is similar to that in European eels (Boesch et al., 2003b) and zebrafish (Boesch et al., 2003a). The formed 3 *N*-glycosylation sites (Asn242, Asn336, and Asn461) are considered to be important for the hydrolysis of ATPase (Figure 1 and 3A). The protein without signal peptides is unlikely to be exposed to the *N*-glycosylation machinery and thus may not be glycosylated *in vivo*, although they contain potential motifs. An important structural ATP-synt_ab domain, nests Pro381, Pro382, Ile383, Asn384, Val385, Leu386, Pro387, Ser388, Leu389, and Ser390, are located in the loop chains and β-sheets forming the binding sites and used as the ATPase proton channel of ion flux across the membrane to drive ATP synthesis (Figure 3A). The ATP-synt_ab (nucleotide-binding) domain is a membrane-binding enzyme complex or an ion transporter that drives the transport of protons across the membrane using ATP hydrolysis. Some transmembrane ATPases also exert their functions in a reversed manner. The function of the ATP-synt_ab has been verified by the extracellular catalytic sector V_1, which is essential for its function of energy transfer to transport substrates across membranes and provide specificity for different substrates (Futai et al., 2000). SMART program analysis revealed 3 typical ATP synthase domains, which are similar to the discovery in *A. anguilla*, *D. rerio*, *O. mykiss*, and *M. zebra* (Figure 2). These results further suggest that AmVHAB1 shares high similarity with one other catadromous fish, and revealed a similar function to AmVHAB1 as VHAB1s in other species. The three-dimensional model of AmVHAB1 showed a significantly similar structure when compared with VHAB1s from *A. anguilla*, *D. rerio*, *O. mykiss*, and *M. zebra*, confirming that AmVHAB1 is related to the process of osmoregulation. The different

α helices, β sheets, and loops in these secondary structures indicate that the specific action mechanisms of the *VHAB1* from the species are different (Figure 3).

In the present study, we compared the mRNA and protein expression changes of V-H$^+$-ATPase over time after the marbled eel in FW was transferred to BW and SW. The results revealed that mRNA and protein expression levels of the gill VHA were significantly higher in the gill tissue of *A. marmorata* acclimated to BW (or SW) than to FW. This is the first study to carefully examine the changes in mRNA and protein expression levels of V-H$^+$-ATPase following the transfer from FW to BW and then to a SW environment. After 1 h of exposure to BW, a 22-fold increase in the level of *AmVHAB1* mRNA was observed. Surprisingly, with an apparent transient 44-fold increase in the *AmVHAB1* mRNA level after 6 h of adaptation to SW, *AmVHAB1* in osmoregulation is a significant challenge to SW during the fast transition. We found that the protein expression level of the gill VHA in the BW-acclimated eel was clearly higher than that in the FW group. Similarly, the protein expression level of SW-acclimated individuals was significantly higher than that in the FW group. Interestingly, the immunoblotting results showed that the protein expression of gill VHA in the BW and SW groups had pronounced expression after 96 h. The time lag between increased mRNA and protein expression was likely because of post-translational modifications and mobilization of intracellular stores to the plasma membrane surface, which typically occur over a much shorter time scale (hours), and the time difference for the *de novo* synthesis of V-H$^+$-ATPase protein. The molecular biological processes of transcription and translation over time and space may have also led to the time inconsistencies between mRNA and protein expression levels of gill VHA. The enhanced *VHAB1* mRNA expression indicated that the V-H$^+$-ATPase protein was expressed highly in gill epithelial cells, suggesting that the gill discharges a large number of ions following exposure to salt water. The basal level of this protein in the SW-acclimated *A. marmorata* gill may be sufficient for driving ion excretion following the exposure to SW. This supports that *AmVHAB1* is involved in the process of osmoregulation in juvenile marbled eel during salinity adaption, and the quick transition in the marbled eel suggests that *AmVHAB1* is more sensitive to salinity changes when compared with other euryhaline fish. The V-H$^+$-ATPase mRNA and protein expression as evaluated by western blotting in Japanese eels also showed a clear increase after the environment transfer from SW to FW (Tse and Wong, 2011). However, the VHA mRNA and protein in gill of *A. marmorata* showed a significant increase during the transfer from FW to SW, indicating that V-H$^+$-ATPase in Japanese eels may have a different molecular mechanism for osmoregulation of AmVHAB1. In zebrafish, as a model organism, higher mRNA expression and protein expression levels were also been detected in free-living zebrafish embryos and larvae exposed to hypo-osmotic conditions (Schredelseker and Pelster, 2004). Based on the results observed in zebrafish and marbled eel, *VHAB1* plays an important role in salinity adaptation during the larval stage of fish. *VHAB1* expression in BW and SW showed no obvious difference compared to the control group within 15 days of seawater exposure (Figure 5). The VHA protein level in BW and SW was upregulated expression when compared with that in FW during the adaptation to 15 days, but the protein expression level after 15 days of exposure to BW and SW were lower than the VHA protein level at 96 h (Figure 6). In euryhaline fish, the consequent activation of the osmoregulatory system contains 2 periods such as the adaptive period and the chronic regulatory period. In the chronic regulatory period, the changed osmotic parameters can return to a new steady state as a result of rest through the osmoregulatory mechanism (Holmes and Donaldson, 1969; Martinez-

Alvarez et al., 2002). In this study, the AmVHAB1 mRNA and protein expression of juvenile marbled eel returned to a new steady state after 15 days of seawater exposure.

In summary, the analysis of the molecular structure and protein model in *A. marmorata* indicated that it was highly homologous to that of other known vertebrate V-H$^+$-ATPases. In this study, we found that the gill V-H$^+$-ATPase B1 isoform plays important roles in the adaptation of elvers to seawater and marine environments. In the present study, juvenile gill AmVHAB1 acclimating to SW showed an identical pattern to the gill Na$^+$/K$^+$-ATPase of Japanese eel during SW acclimation (Tang et al., 2012). *AmVHAB1* was expressed in juvenile *A. marmorata* and the time-course experiments revealed the transient change in *VHAB1* expression in the elvers. The 22-44% upregulated expression of *VHAB1* in the gill indicated that the elvers mainly depend on the gill to adapt to salinity changes, and VHA in the gill may play a more important role in activating the ion excretion model for juvenile *A. marmorata* than in adult eels. However, further studies examining the adaptation to SW during long-term growth of juvenile *A. marmorata* requires further investigation. The exact role of gill V-H$^+$-ATPase and the mechanisms regulating its expression in this process remain unclear and further studies are needed.

ACKNOWLEDGMENTS

Supplementary material

REFERENCES

Boesch ST, Eller B and Pelster B (2003a). Expression of two isoforms of the vacuolar-type ATPase subunit B in the zebrafish *Danio rerio*. *J. Exp. Biol*. 206: 1907-1915.

Boesch ST, Niederstätter H and Pelster B (2003b). Localization of the vacuolar-type ATPase in swimbladder gas gland cells of the European eel (*Anguilla anguilla*). *J. Exp. Biol*. 206: 469-475.

Bowman BJ, Vazquez-Laslop N and Bowman EJ (1992). The vacuolar ATPase of *Neurospora crassa*. *J. Bioenerg. Biomembr*. 24: 361-370.

Cutler CP and Cramb G (2001). Molecular physiology of osmoregulation in eels and other teleosts: the role of transporter isoforms and gene duplication. *Comp. Biochem. Physiol. A Mol. Integr. Physiol*. 130: 551-564.

Forgac M (2007). Vacuolar ATPases: rotary proton pumps in physiology and pathophysiology. *Nat. Rev. Mol. Cell Biol*. 8: 917-929.

Futai M, Oka T, Sun-Wada G, Moriyama Y, et al. (2000). Luminal acidification of diverse organelles by V-ATPase in animal cells. *J. Exp. Biol*. 203: 107-116.

Holmes WN and Donaldson EM (1969). The body compartments and the distribution of electrolytes. *Fish Physiol*. 1: 1-89.

Jefferies KC and Forgac M (2008). Subunit H of the vacuolar (H$^+$) ATPase inhibits ATP hydrolysis by the free V$_1$ domain by interaction with the rotary subunit F. *J. Biol. Chem*. 283: 4512-4519.

Jefferies KC, Cipriano DJ and Forgac M (2008). Function, structure and regulation of the vacuolar (H$^+$)-ATPases. *Arch. Biochem. Biophys*. 476: 33-42.

Leng XH, Manolson MF and Forgac M (1998). Function of the COOH-terminal domain of Vph1p in activity and assembly of the yeast V-ATPase. *J. Biol. Chem*. 273: 6717-6723.

Livak KJ and Schmittgen TD (2001). Analysis of relative gene expression data using real-time quantitative PCR and the $2^{-\Delta\Delta Ct}$ method. *Methods* 25: 402-408.

Martinez-Alvarez RM, Hidalgo MC, Domezain A, Morales AE, et al. (2002). Physiological changes of sturgeon *Acipenser naccarii* caused by increasing environmental salinity. *J. Exp. Biol*. 205: 3699-3706.

Moriyama Y, Hayashi M, Yamada H, Yatsushiro S, et al. (2000). Synaptic-like microvesicles, synaptic vesicle counterparts in endocrine cells, are involved in a novel regulatory mechanism for the synthesis and secretion of hormones. *J. Exp. Biol*. 203: 117-125.

Nelson N (2003). A journey from mammals to yeast with vacuolar H+-ATPase (V-ATPase). *J. Bioenerg. Biomembr*. 35: 281-289.

Niederstatter H and Pelster B (2000). Expression of two vacuolar-type ATPase B subunit isoforms in swimbladder gas gland cells of the European eel: nucleotide sequences and deduced amino acid sequences. *Biochim. Biophys. Acta* 1491: 133-142.

Perry SF, Beyers ML and Johnson DA (2000). Cloning and molecular characterisation of the trout (*Oncorhynchus mykiss*) vacuolar H($^+$)-ATPase B subunit. *J. Exp. Biol*. 203: 459-470.

Reilly BD, Cramp RL, Wilson JM, Campbell HA, et al. (2011). Branchial osmoregulation in the euryhaline bull shark, *Carcharhinus leucas*: a molecular analysis of ion transporters. *J. Exp. Biol*. 214: 2883-2895.

Schredelseker J and Pelster B (2004). Isoforms vatB1 and vatB2 of the vacuolar type ATPase subunit B are differentially expressed in embryos of the zebrafish (*Danio rerio*). *Dev. Dyn*. 230: 569-575.

Seidelin M, Madsen SS, Cutler CP and Cramb G (2001). Expression of gill vacuolar-type H+-ATPase B subunit, and Na+, K+-ATPase α1 and β1 subunit messenger RNAs in smolting *Salmo salar*. *Zoolog. Sci*. 18: 315-324.

Shiao JC, Iizuka Y, Chang CW and Tzeng WN (2003). Disparities in habitat use and migratory behavior between tropical eel *Anguilla marmorata* and temperate eel *A. japonica* in four Taiwanese rivers. *Mar. Ecol. Prog. Ser*. 261: 233-242.

Tang CH, Lai DY and Lee TH (2012). Effects of salinity acclimation on Na($^+$)/K($^+$)-ATPase responses and FXYD11 expression in the gills and kidneys of the Japanese eel (*Anguilla japonica*). *Comp. Biochem. Physiol. A Mol. Integr. Physiol*. 163: 302-310.

Tse WKF and Wong CKC (2011). nbce1 and H+–atpase mRNA expression are stimulated in the mitochondria-rich cells of freshwater-acclimating Japanese eels (*Anguilla japonica*). *Can. J. Zool*. 89: 348-355.

Wang L, Wang WN, Liu Y, Cai DX, et al. (2012). Two types of ATPases from the Pacific white shrimp, *Litopenaeus vannamei* in response to environmental stress. *Mol. Biol. Rep*. 39: 6427-6438.

Wieczorek H, Brown D, Grinstein S, Ehrenfeld J, et al. (1999). Animal plasma membrane energization by proton-motive V-ATPases. *Bioessays* 21: 637-648.

Wu C and Hamada M (2000). Experiments: planning, analysis, and parameter design optimization. John Wiley & Sons, New York.